

RESEARCH

Open Access



# Prion protein regulates invasiveness in glioblastoma stem cells

Mariana B. Prado<sup>1†</sup>, Bárbara P. Coelho<sup>1†</sup>, Rebeca P. Iglesia<sup>1</sup>, Rodrigo N. Alves<sup>1</sup>, Jacqueline M. Boccacino<sup>1</sup>, Camila F. L. Fernandes<sup>1</sup>, Maria Isabel Melo-Escobar<sup>1</sup>, Shamini Ayyadhury<sup>2,3</sup>, Mario C. Cruz<sup>4</sup>, Tiago G. Santos<sup>5</sup>, Flávio H. Beraldo<sup>6,7</sup>, Jue Fan<sup>6</sup>, Frederico M. Ferreira<sup>8</sup>, Helder I. Nakaya<sup>9,10,11</sup>, Marco A. M. Prado<sup>6,7</sup>, Vania F. Prado<sup>6,7</sup>, Martin L. Duenwald<sup>7</sup> and Marilene H. Lopes<sup>1\*</sup>

## Abstract

**Background** Glioblastoma (GBM) is an aggressive brain tumor driven by glioblastoma stem cells (GSCs), which represent an appealing target for therapeutic interventions. The cellular prion protein (PrP<sup>C</sup>), a scaffold protein involved in diverse cellular processes, interacts with various membrane and extracellular matrix molecules, influencing tumor biology. Herein, we investigate the impact of PrP<sup>C</sup> expression on GBM.

**Methods** To address this goal, we employed CRISPR-Cas9 technology to generate PrP<sup>C</sup> knockout (KO) glioblastoma cell lines, enabling detailed loss-of-function studies. Bulk RNA sequencing followed by differentially expressed gene and pathway enrichment analyses between U87 or U251 PrP<sup>C</sup>-wild-type (WT) cells and PrP<sup>C</sup>-knockout (KO) cells were used to identify pathways regulated by PrP<sup>C</sup>. Immunofluorescence assays were used to evaluate cellular morphology and protein distribution. For assessment of protein levels, Western blot and flow cytometry assays were employed. Transwell and growth curve assays were used to determine the impact of loss-of-PrP<sup>C</sup> in GBM invasiveness and proliferation, respectively. Single-cell RNA sequencing analysis of data from patient tumors from The Cancer Genome Atlas (TCGA) and the Broad Institute of Single-Cell Data Portal were used to evaluate the correspondence between our in vitro results and patient samples.

**Results** Transcriptome analysis of PrP<sup>C</sup>-KO GBM cell lines revealed altered expression of genes associated with crucial tumor progression pathways, including migration, proliferation, and stemness. These findings were corroborated by assays that revealed impaired invasion, migration, proliferation, and self-renewal in PrP<sup>C</sup>-KO GBM cells, highlighting its critical role in sustaining tumor growth. Notably, loss-of-PrP<sup>C</sup> disrupted the expression and localization of key stemness markers, particularly CD44. Additionally, the modulation of PrP<sup>C</sup> levels through CD44 overexpression further emphasizes their regulatory role in these processes.

**Conclusions** These findings establish PrP<sup>C</sup> as a modulator of essential molecules on the cell surface of GSCs, highlighting its potential as a therapeutic target for GBM.

**Keywords** Cellular prion protein, Glioblastoma stem cells, CD44, Invasion, Migration

<sup>†</sup>M.B. Prado and B.P. Coelho contributed equally to this work.

\*Correspondence:  
Marilene H. Lopes  
marileneh@usp.br

Full list of author information is available at the end of the article



## Background

Glioblastoma (GBM) is a highly invasive and aggressive tumor of the central nervous system that differs from other adult-type diffuse gliomas since it expresses the wild-type form of isocitrate dehydrogenase (IDH) [1]. It shows a diffuse growth pattern, which hinders its complete surgical removal and contributes to its high recurrence rates [2, 3]. Another reason for recurrence is a small subpopulation of stem-like cells, denominated GBM stem cells (GSCs) [4], which are resistant to conventional therapy, present self-renewal and tumor initiation abilities, and are the main source of tumor cell heterogeneity [5]. GSCs exhibit plasticity and can transition between different cellular states, therefore being difficult to identify by specific molecular markers. Nevertheless, many of GSCs' features resemble neural stem cells, such as the expression of CD44, CD133, CD24, EGFR, and SOX2, which may aid in their identification in the tumor bulk [5–8]. Additionally, GSCs reside in four distinct niches: perivascular, hypoxic, necrotic, and invasive [9, 10]. The tumor microenvironment determines the manifestation of diverse GSCs phenotypes, leading to spatially distributed intra-tumoral heterogeneity within individual patients. Given these specific characteristics of GBM biology, there is still only a limited number of treatments that present any effects against this disease [11]. Indeed, even though it was licensed in 1999, temozolomide (TMZ) is still the standard chemotherapeutic agent used to date [12, 13]. Therefore, the pursuit of a novel therapeutic target is indispensable for the development of more efficient treatments.

Cell surface molecules represent potential targets for therapies against GBM due to their accessibility and implication in critical signaling transduction. The cellular prion protein (PrP<sup>C</sup>), a glycosyl-phosphatidylinositol (GPI)-anchored protein, is found on the plasma membrane and is highly expressed in nervous system cells [14]. Interestingly, PrP<sup>C</sup> is associated with the formation and modulation of multiprotein complexes containing different ligands related to neural plasticity processes [15], and, therefore, has an essential function as a scaffold protein, creating dynamic signaling platforms on the cell surface of distinct neural cells [16, 17].

Several PrP<sup>C</sup> ligands participate in cell adhesion and migration processes, such as cell neural adhesion molecule 1 (NCAM1), laminin, and laminin receptors (reviewed in [18]). Additionally, many studies demonstrate that PrP<sup>C</sup> can co-localize and interact with several stemness modulators on the cell surface [18, 19]. For example, PrP<sup>C</sup> can interact with CD44 in resistant breast cancer, modulating proteins involved in the cell cycle and cell motility [20]. CD44 is a well-known cancer stem-like cell marker involved in cell migration and cell survival [21], and it is known to modulate cell growth

and stemness in GBM [22]. Interestingly, CD44 has a pivotal role in the collective invasion of luminal breast cancer [23] and its knockdown in colorectal cancer leads to impaired cell motility and invasion [24]. PrP<sup>C</sup> also participates in the intracellular trafficking of CD133, an important stem cell marker, since copper-mediated endocytosis of PrP<sup>C</sup> stimulates CD133 internalization [19]. Expression of PrP<sup>C</sup> is highly related to tumorigenesis and maintenance of different types of tumors, such as breast cancer, colorectal cancer, and neuroblastoma [25–27], being also involved in protection against apoptosis [17]. In GBM, data from the literature shows that PrP<sup>C</sup> knockdown significantly inhibits *in vivo* tumorigenesis [28]. Furthermore, PrP<sup>C</sup> modulates cell migration and invasion in melanomas, breast and lung cancer, among others [18, 29, 30]. Data from our group has also shown that knocking down PrP<sup>C</sup> downregulates the expression of proteins involved in cell motility *in vitro*, as well as decreases cell growth and increases overall survival *in vivo* [19, 31]. Given the invasive profile of GBM and the plethora of PrP<sup>C</sup> partners implicated in cell motility and invasion, a more in-depth study of our model could shed light on novel therapeutic avenues.

Numerous studies have highlighted the role of PrP<sup>C</sup> as a scaffold protein capable of forming multiprotein complexes, influencing critical tumorigenic pathways, and interacting with established cancer markers [16, 17, 32]. However, the precise impact of PrP<sup>C</sup> on GBM invasiveness remains unclear. To address this gap, we generated GBM PrP<sup>C</sup> knockout (KO) cells by CRISPR-Cas9 gene editing, and investigated PrP<sup>C</sup>'s role in GBM and GSCs biology, with a focus on GBM's proliferative, migratory, and invasive capacities.

## Methods

### Cell culture

Glioblastoma U87 (RRID: CVCL\_0022) and U251 (RRID: CVCL\_0021) cell lines were purchased from the American Type Culture Collection (ATCC) and stored in our cell culture facility. All media used for cell culture were purchased from Thermo Fisher Scientific unless stated otherwise. Cells were cultured in monolayer condition using Dulbecco's Modified Eagle Medium (DMEM, Thermo Fisher Scientific, #31600034) supplemented with 10% fetal bovine serum (FBS), which was replaced every two days. To enrich the cell culture with GSCs, the GBM cell lines were grown as neurospheres with DMEM-F12 media (Thermo Fisher Scientific, #12500062) supplemented with 2% B27, 20ng/ml Epidermal Growth Factor (EGF, Sigma, E9644#), and 20ng/ml basic Fibroblast Growth Factor (bFGF, Sigma, #SRP3043). This well-established protocol is widely recognized for promoting the expression of stem cell markers and supporting neurosphere formation in glioma cultures [33, 34].

### Knockout of PrP<sup>C</sup> gene

We generated PrP<sup>C</sup>-KO cells following Dr. Zhang's protocol (<https://www.addgene.org/crispr/zhang>), and used the human PrP<sup>C</sup> gene sequence (*PRNP*, NM\_000311.3) to create gRNA sequences using optimized CRISPR Design (<http://crispr.mit.edu/>). The following sequences were inserted in a px330-U6-GFP vector plasmid [35]: Hu *PRNP* Top1 CACCGgctggggcagccgatacccg and Hu *PRNP* Bottom1 AAACcgggtatcgctgccccagcC, following the manufacturer's instructions. To ensure on-target accuracy, we utilized IDT's CRISPR gRNA checker to perform thorough off-target analysis, which confirmed high specificity of our gRNA sequence. Additionally, we conducted a BLAST analysis that demonstrated 100% alignment of the gRNA with the *PRNP* gene, further verifying our target accuracy. Cells were transfected using Lipofectamine 2000 following the manufacturer's protocol. Cells were later selected using 0.5 µg/ml puromycin for 2 days. Selected cells were detached, and 400 cells were added in 200 µl of media and seeded in one well of a 96-well plate. Starting from the first well, 100 µl of media was transferred into the next well, which was then complemented with 100 µl of media and so on successively. Wells containing only one cell at the end of the process were labeled, and after a few weeks, the expression of PrP<sup>C</sup> protein from the clones obtained was tested via western blot and flow cytometry assays.

### Bulk RNA-Seq

RNA was extracted using the RiboPure RNA Purification (Thermo Fisher Scientific) kit, following the manufacturer's instructions. RNA-Seq libraries were made by an outsourced service (Indegene) using Illumina Stranded mRNA Prep (Illumina). The prepared libraries were sequenced using the Illumina NextSeq 500 platform (Illumina). Libraries were sequenced to an average depth of 40 million reads per sample. FastQC was used to check the quality of the raw sequence data. Cutadapt was used for trimming, while TopHat and Bowtie were used for the alignment against the GRCh38.100 human genome reference. Data analysis was done with an outsourced service, Duna Bioinformatics. DESeq2 was used for differential analysis with the WT versus PrP<sup>C</sup>-KO groups, with a value of  $p < 0.05$  and/or  $\log_2\text{foldchange} \leq -2$  and  $\geq 2$  being considered to filter the statistically significant differentially expressed genes (DEGs). DEGs were subjected to functional profiling with clusterProfiler: the enrichment analysis was performed for the categories biological processes, cellular components, molecular functions, and KEGG. A threshold of adjusted p-value  $\leq 0.05$  was used to define significantly enriched terms.

### Sequencing of the PrP<sup>C</sup> gene (*PRNP*)

DNA lysis buffer (Tris 50 mmol; EDTA 2.5 mmol, 0.1% SDS, 4 mmol NaCl, pH 8.0) and 10 µL proteinase K were added to the cells in separate tubes, which were then incubated at 55°C for 1 hour. After cell lysis, an equal volume of Phenol: Chloroform: Iso-Amyl alcohol was added, and the tubes were gently inverted for 5 minutes. Following centrifugation, the top aqueous phase was carefully transferred to a new tube. DNA was then precipitated with isopropanol, centrifuged, and the supernatant discarded. The resulting pellet was washed with 70% ethanol, centrifuged, and allowed to air-dry for 10 minutes in the hood. Finally, the pellet was resuspended in PCR-grade water, and the DNA concentration was measured using NanoDrop. Purified genomic DNA (20 ng/µL) was amplified using Taq DNA Polymerase (Thermo Fisher) according to the manufacturer's protocol. To sequence the PrP<sup>C</sup> gene (*PRNP*), the following primers were used: Forward 5'-AGAAGTACAGGGTGGCAACA-3' and Reverse 5'-GACCGTGTGCTGCTTGATTG-3'. The PCR products were submitted for sequencing at Robarts Research Institute in London, Canada. Sequence data were analyzed with FinchTV, Clustal Omega (<https://www.ebi.ac.uk/Tools/msa/clustalo/>), and ORFinder (<https://www.ncbi.nlm.nih.gov/orffinder/>).

### RT-qPCR

mRNA samples were obtained using Aurum Total RNA Fatty and Fibrous Tissue Kit or RiboPure™ RNA Purification Kit (Thermo Fisher Scientific), following the manufacturer's protocol. The concentration of the samples was measured using Nanodrop or Epoch. cDNA was obtained using an Applied Biosystem High-Capacity cDNA Reverse Transcription Kit from RNA (1 µg of RNA) or SuperScript™ III Reverse Transcriptase (2 µg of RNA; Invitrogen) following the manufacturer's instructions. qPCR was performed using SYBR Green Master Mix (Thermo Fischer Scientific, #4472908) and the primers used are described in Table 1. The delta-delta-Ct method [36] was used to compare gene expression between the groups, with TBP as the reference gene.

### Western blotting

Cells were seeded in 6-well plates, and, on the following day, protein extracts were obtained using RIPA buffer (50 mM Tris HCL, 150 mM NaCl, 1% Triton X-100, 0.1% sodium dodecyl sulfate and 1 mM EDTA, 1% sodium deoxycholate) with protease and phosphatase inhibitors. Total protein was quantified using Pierce BCA Protein Assay Kit (Thermo Fisher Scientific, #23227) or Quick Start™ Bradford 1x Dye Reagent (Bio-Rad). Protein extracts, along with a protein ladder (Thermo Fisher catalog #26619), were separated using SDS-PAGE and transferred to a PVDF membrane. The membrane was

**Table 1** Primers used for RT-qPCR analysis

Gene	Forward Primer sequence (5'-3')	Reverse Primer sequence (5'-3')
<i>ABCBS</i>	ATTGGAGTGGTTAGTCAAGAGCC	AGTCACATCATCTCGTCCATACT
<i>CD24</i>	CTCCTACCCACGCAGATTATTC	AGAGTGAGACCACGAAGAGAC
<i>CD44</i>	ACAGTACAGCCATTATGCAAGG	TTCCCCACTTCTCAAACATTCT
<i>DOT1L</i>	CTGCCGGTCTACGATAAACATC	AGCTTGAGATCCGGGATTCT
<i>EGF</i>	TGTCCACGCAATGTGTCTGAA	CATTATCGGGTGAGGAACAACC
<i>EGFR</i>	CAGACCCGGACGACAGGC	ATACTGGACGGAGTCAGGGG
<i>EPHA4</i>	ACTTGAAGGCGTGGTCACT	CCCAGACCCAATGCCACGAA
<i>EPHB4</i>	CTCCTTCCTGCGGTAAACG	GGACGTAGCTCATCTCGGCA
<i>LAMAS</i>	GGCTTTCCCGAGCTGTACT	AGGGTCCCACCGTAGGATGA
<i>NCAM1</i>	CAGCCAGTCCAAGGGGAACC	ACGGGAGCCTGATCTCTGGT
<i>CD133</i>	ACCAGGTAAGAACCCGGATCAA	CAAGAATCCCGCTCTAGCACT
<i>PRNP</i> after deletion	ATGAGCCGTTGCTAATGCCA	GCCAGAGGTATCCAGGCAAA
<i>PRNP</i> before deletion	GGGACCCAGTGAGGAGG	TGCTCTGAAAAGCGAAGCCA
<i>PRNP</i> in deletion	CCTGGAGGCAACCGTACT	TGGCTTGTTCCTACTGACTG
<i>SOCS3</i>	GCCACCTACTGAACCCTCCT	ACGGTCTCCGACAGAGATG
<i>SOX2</i>	ATGCACCGCTACGACG	CTTTTGCACCCTCCCATTT
<i>SOX9</i>	AGGTGCTCAAAGGCTACGACT	AGATGTGCGTCTGCTCCGTG
<i>TBP</i>	AGGATAAGAGAGCCACGAACCA	CTTGCTGCCAGTCTGGACTGT
<i>THBS2</i>	AGCTCCTCTTCAATCCCCGC	AGGGCTCACCTCTCCATTG
<i>TIMP3</i>	CTTCGGCAGCTGGTCTACA	GCCATCATAGACGCGACCTGT
<i>WNT10B</i>	GTGAGCGAGACCCCACTATG	CACTCTGTAACCTTGCACTCATC

blocked with 5% bovine serum albumin (BSA, Sigma) in Tris-Buffered Saline with 0.1% Tween® 20 Detergent (TBST) for 1 h. To optimize the experimental workflow, the membranes were horizontally cut prior to hybridization with the primary antibodies at the concentration of 1:1000 for mouse CD44 (#3570S, Cell Signaling Technology) or mouse PrP<sup>C</sup> 3F4 (MAB1562, Millipore), and 1:8000 for rabbit GAPDH (Cell Signaling Technology, #5174) in 5% BSA in TBST at 4° C. Secondary antibodies used were anti-rabbit HRP (Cell Signaling Technology, #7074) or anti-mouse HRP (Cell Signaling Technology, #7076) in a concentration of 1:5000. Chemiluminescent detection was performed using the Imaging System (Amersham Imager 600) or exposure to hyperfilm. All antibodies used in this study are highly specific and detect the expected bands as indicated in their respective datasheets. Protein bands from Western blot experiments were quantified using densitometry. For densitometry, we utilized the ImageLab (BioRad) software (version 6.1) with the Gel Analysis function to quantify band intensity. Protein expression levels were normalized to the corresponding loading control (HSP90, GAPDH or  $\beta$ -actin), and relative intensities were calculated by comparing each sample to the control condition. In the overexpression experiments for CD44 and PrP<sup>C</sup>, control samples were loaded on separate membranes and triplicates for the transfected cells were run on the same gel, ensuring consistent experimental conditions across the treated samples. The resulting values were analyzed statistically using R with the ggplot2 package for visualization.

### Flow cytometry

Neurospheres were dissociated, and 10<sup>6</sup> cells for each condition were washed with PBS and blocked with 5% BSA in PBS for 30 min on ice. Cells were then incubated with the primary antibodies anti-PrP<sup>C</sup> (ab703, Abcam), anti-CD44 (#3570, Cell Signaling Technology), anti-CD133 (Cell Signaling Technology, #64326), anti-SSEA1 (Cell Signaling Technology, #4744S) 1:50 in 0.5% BSA in PBS for 30 min on ice, following a wash with PBS. The pellet was then resuspended in secondary antibodies anti-mouse Alexa Fluor 488 (Invitrogen, #A28175) or anti-rabbit Alexa Fluor 647 (Invitrogen, #A27040) for 30 min on ice. After washing, cells were resuspended in 300  $\mu$ L of 0.5% BSA in PBS and analyzed by flow cytometry in a FACSCanto II (BD Biosciences) Flow Cytometer. For controls, cells were incubated with only the secondary antibody.

### Cell growth curve

Cells (2.5  $\times$  10<sup>4</sup>) in DMEM/F-12 medium supplemented with growth factors were seeded in triplicate in P6-well plates. Cell counting started 2 days post-seeding. Cells were detached daily using 0.25% trypsin (Gibco, #25200-056) in HBSS (Gibco, #14170-112) and counted for 5 consecutive days using a Neubauer chamber.

### Self-renewal

Neurospheres were dissociated with 0.25% trypsin (Gibco, #25200-056, Gibco) in HBSS (Gibco, #14170-112) and then counted. In triplicate, 200 cells were

seeded into 96-well plates and cultured for 10 days, with fresh medium added every 48 h. At the end of the growth period, images of each well were captured using a Zeiss PrimoVert microscope, and both the number and size of the neurospheres were evaluated according to protocol [33, 34].

#### Extreme limiting dilution assay (ELDA)

U87 WT and PrP<sup>C</sup> KO cells were dissociated into single-cell suspensions with Accutase StemPro (Gibco, #A1110501) and resuspended in neurosphere medium. After counting, cells were seeded in 96-well plates at densities of 1, 20, 50, or 100 cells per well, with 24 replicates per condition. After 9 days, four images per well were captured at 4× magnification using the EVOS XL Core microscope. Neurospheres larger than 50 μm were counted, and the data was analyzed using ImageJ software and entered into the ELDA software (<http://bioinf.wehi.edu.au/software/elda/>).

#### Immunofluorescence

Cells were seeded on poly-L-lysine-coated coverslips and allowed to attach overnight. The next day, cells were fixed with 4% paraformaldehyde (PFA) and blocked in phosphate-buffered saline (PBS) containing 10% normal goat serum and 0.2% Triton X-100 for 1 h at 4 °C. Primary antibodies for CD44 (Cell Signaling Technology, #3570) and PrP<sup>C</sup> (Abcam, ab703) were applied at a 1:500 dilution in PBS with 2% normal goat serum and 0.2% Triton X-100 and incubated overnight. The following day, coverslips were washed three times with PBS, then incubated for 1 h with Alexa Fluor 633 anti-rabbit (#A-21071, Invitrogen) or Alexa Fluor 488 anti-mouse (#A28175, Invitrogen) secondary antibodies at a 1:1000 dilution, along with DAPI (Abcam, ab228549) at 1:1000, all in PBS with 2% normal goat serum and 0.2% Triton X-100. Coverslips were then washed three times with PBS and mounted using ProLong Gold Antifade (Thermo Scientific). Images were acquired with a Leica SP5 or SP8 microscope.

#### Colocalization analysis

Colocalization analysis was conducted using CellProfiler (version 4.2.6) with a pipeline comprising the following modules: GaussianFilter, Threshold, Watershed, ImageMath, ConvertImageToObjects, MeasureObjectSizeShape, FilterObjects, MeasureObjectIntensity, MeasureColocalization, and ExportToSpreadsheet. Images were processed as 3D grayscale stacks, with channels labeled according to fluorescence: DAPI (nuclei), CD44 (488 nm), and PrP<sup>C</sup> (647 nm). To reduce noise, Gaussian smoothing ( $\sigma=1$ ) was applied, followed by global thresholding using Minimum Cross-Entropy for nuclei and Otsu's method for CD44. Nuclei segmentation was achieved through the watershed method, while

cytoplasmic segmentation was accomplished via image subtraction using the ImageMath module. Objects were filtered based on a minimum size of >10,000 px<sup>3</sup>, and CD44 and PrP<sup>C</sup> intensities within the cytoplasm were measured. Colocalization between CD44 and PrP<sup>C</sup> was analyzed with the MeasureColocalization module, calculating correlation based on pixel intensity values within the cytoplasm. Pearson's correlation coefficient assessed the linear relationship between CD44 and PrP<sup>C</sup> intensity distributions, with normalized intensity values prior to correlation calculation. A threshold set at 20% of maximum intensity excluded low-intensity pixels. The resulting correlation values indicate the degree of overlap between the two signals within each object, where higher values represent stronger colocalization.

The resulting values were analyzed statistically using R with the ggplot2 package for visualization. The pipeline is available on GitHub under the name *Correlation\_pipeline.ccpipe* (<https://github.com/marilenehohmuth/PrionGBM>).

#### Cell transfection

U87 glioblastoma (GBM) cells were transfected using Lipofectamine 2000 (Thermo Fisher Scientific, #11668-019) according to the manufacturer's protocol. To induce CD44 overexpression, we utilized the CD44 cDNA ORF clone fused with GFP (Sino Biological, Cat. No. HG12211-ACG). To overexpress PrP<sup>C</sup>, we used the pcDNA3.1-GFP-tagged PrP<sup>C</sup> plasmid, a construct kindly provided by our collaborator, Dr. Vilma Regina Martins, that encodes both the human *PRNP* gene and GFP.

#### Cell migration and invasion assays

For migration assays, cells were plated on the upper chamber of transwell inserts (Greiner Bio-one, #662638) with culture medium without FBS, while medium with FBS was added to the well to serve as a chemoattractant. Cells were cultured in 5% CO<sub>2</sub> at 37 °C for 24 h. Next, cells were fixed by adding 4% PFA to both the well and upper chamber and then washed with PBS. Cells were stained using hematoxylin and eosin (H&E) for 20 min and then photographed in 4 random fields for quantification. For invasion assays, prior to cell plating, the upper chamber of transwell inserts (662 638, Greiner Bio-one) was coated with Geltrex (A1413302, Thermo Fisher Scientific), which was left to polymerize for 1 h in the cell incubator. Afterward, excess non-polymerized Geltrex was removed, and cells were plated on top with culture medium without FBS, while medium with FBS was added to the well to serve as a chemoattractant. Cells were cultured in 5% CO<sub>2</sub> at 37 °C for 24 h. Subsequently, cells were fixed by adding 4% PFA to both the well and upper chamber and then washed with PBS. Cells were stained using H&E or crystal violet for 20 min and then

photographed in 4 different random fields for quantification. Image analysis for counting migrating cells after CD44 transfection in a transwell assay was performed using CellProfiler 4.2.6, with a pipeline incorporating the modules: CorrectIlluminationCalculate, CorrectIlluminationApply, ColorToGray, RunCellpose, OverlayOutlines, SaveImages, and ExportToSpreadsheet. The CorrectIlluminationCalculate module was used to create an illumination correction image, which was then applied via CorrectIlluminationApply to normalize image intensity. Images were converted to grayscale with ColorToGray to optimize cell detection. Cell segmentation was accomplished using the RunCellpose module with a custom model trained in Cellpose 2.2.3 on five annotated images representative of the assay's cell morphology. Quantitative data, including cell counts, were exported using ExportToSpreadsheet for further analysis. The CellProfiler pipeline, custom Cellpose model, and a sample image are available in the supplementary data and on GitHub (<https://github.com/marilenehohmuth/PrionGBM>) for reproducibility.

#### Analysis of single-cell RNA sequencing data obtained from patient samples

Public data were obtained from the Broad Institute Single-Cell Data Portal ([https://singlecell.broadinstitute.org/single\\_cell/study/SCP503](https://singlecell.broadinstitute.org/single_cell/study/SCP503)). The metadata obtained contained information about cell expression patterns and culture methods used to generate t-distributed stochastic neighbor embedding graphics. Data were scaled, and using the find signatures function, we delimited the markers related to each cluster. Selected clusters had their pattern of expression further analyzed using gene set analysis.

#### Correlation analysis between CD44 and *PRNP* expression in GBM samples

To assess the relationship between CD44 and *PRNP* expression levels in glioblastoma (GBM) samples, we utilized RNA sequencing data from The Cancer Genome Atlas (TCGA). After acquiring the data, we performed normalization using the TMM method from the edgeR package in R, filtering out low-expression genes. A scatter plot was generated to visualize the correlation, with CD44 expression on the y-axis and *PRNP* expression on the x-axis, where each point represented an individual GBM sample. We calculated the best-fit linear regression using the `lm()` function and determined the Pearson correlation coefficient ( $r$ ) along with its significance ( $p$ -value) using a two-tailed test. The resulting scatter plot was created with `ggplot2`, displaying the correlation coefficient and  $p$ -value in the top left corner.

#### Statistical analysis

All statistical analyses were conducted using R version 4.1.3 (2022-03-10) and RStudio (version 2022.02.1). When comparing two groups that adjust to a normal distribution, the Student's t-test was used. For multiple comparisons, we used One- or Two-way analysis of variance (ANOVA) with Tukey's or Bonferroni's post-hoc tests. A value of  $p < 0.05$  was considered statistically significant. Kaplan-Meier survival curves were used and the two-sided log rank test was utilized to compare the survival curves. Pearson's or Spearman's correlation coefficients were calculated as appropriate to evaluate relationships between variables, and linear regression was applied where relevant.

#### Results

##### Knockout of PrP<sup>C</sup> decreases stemness and proliferation of glioblastoma cells

To better understand the role of PrP<sup>C</sup> in the biology of GBM, PrP<sup>C</sup> knockout (PrP<sup>C</sup>-KO) glioblastoma cell lines (U87 and U251) were generated by the CRISPR-Cas9 system (Fig. 1a) and cultured in monolayer and neurosphere conditions enriched with stem-like cells [19]. To evaluate *PRNP* gene editing, we designed sets of primers flanking different regions of the *PRNP* sequence, based on the designed gRNA: before the deletion, in the deletion site, and after the deletion. In U87 cells, mRNA sequence in the region of the predicted deletion was not detected on KO cells (Fig. 1b). A remaining expression of the mRNA sequence of the *PRNP* gene was detected in both the before and after deletion site (Additional Fig. 1a-c). The residual expression found in the after deletion site and the higher levels detected in the before the deletion site could be due to the direction (3' to 5') by which mRNA starts to be degraded by the molecular machinery. A deletion of 223 bp was found in two different clones (Additional Fig. 1c), confirming the precision of the CRISPR-Cas9 gene editing. Moreover, U87 WT cells cultured as neurospheres (N), which exhibit enhanced GSCs markers [19], showed significant increased expression of *PRNP* when compared with the monolayer (M) condition (Fig. 1b).

We also confirmed the deletion of the *PRNP* gene by the lack of PrP<sup>C</sup> protein expression in KO cells (Fig. 1c-d). Noteworthy, *PRNP* increase in neurospheres was also observed in protein levels for both cell lines (Fig. 1c), suggesting that PrP<sup>C</sup> has an essential role in cells with stem-like features. Indeed, loss-of-PrP<sup>C</sup> affected the expression of stem cell markers (Fig. 1e). In U87 cells grown as monolayers, PrP<sup>C</sup> KO reduced the expression of *SOX2* ( $p < 0.0001$ ), while it increased the expression of *CD133* ( $p = 0.0083$ ). Expression of *SOX2* ( $p < 0.0001$ ), *CD44* ( $p = 0.0003$ ), and *SOCS3* (0.0014) increased in WT neurosphere condition in comparison to WT monolayer, while

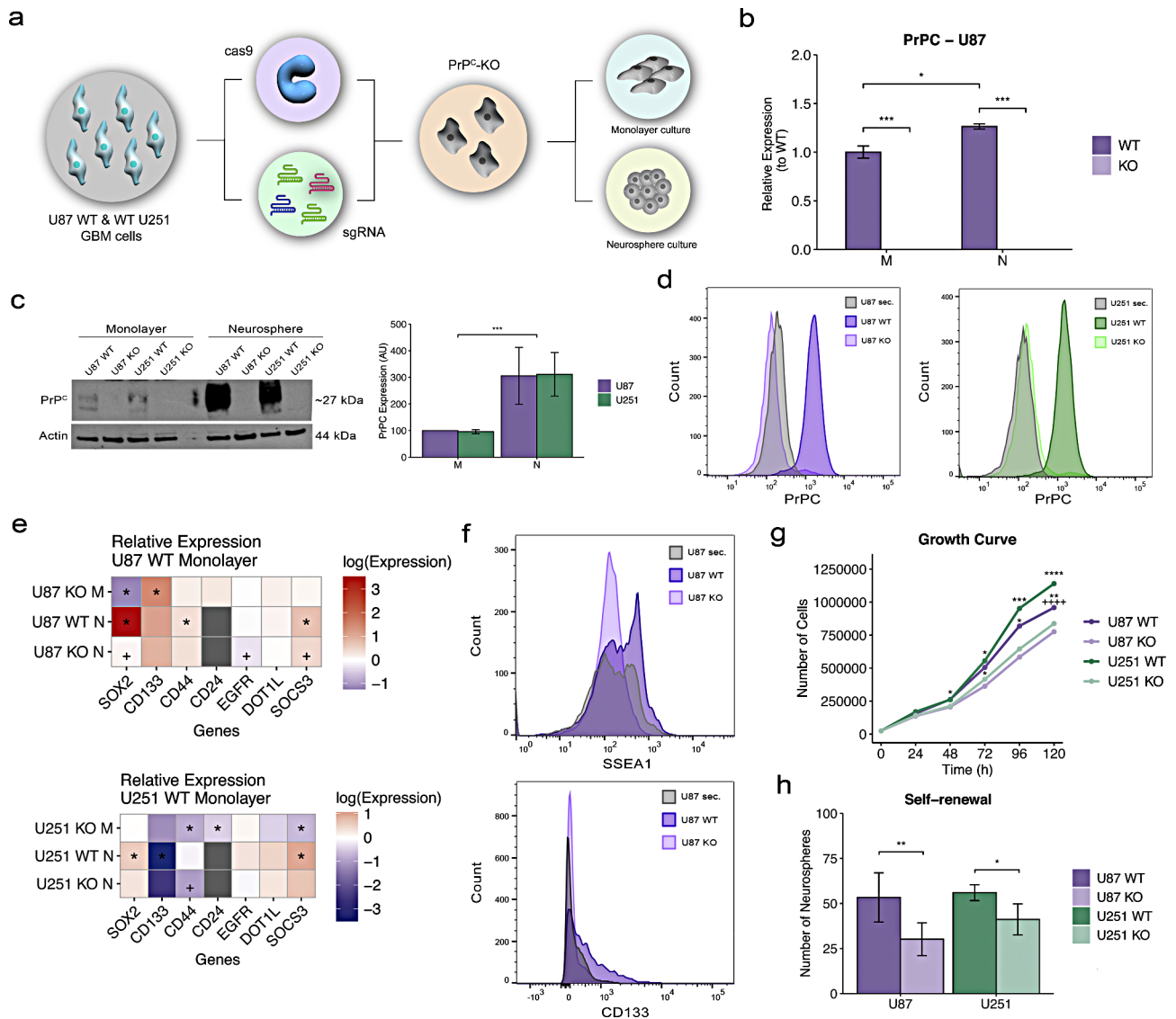


**Fig. 1** Characterization of U87 and U251 PrP<sup>C</sup> KO cells. **(a)** Illustration of the study design for the generation of PrP<sup>C</sup> KO cells. **(b)** RT-qPCR of *PRNP* mRNA amplifying the region inside the deletion site (inDEL) in U87 cells ( $n=4$ ;  $**P<0.01$ ;  $****P<0.0001$ ). **(c)** Expression of PrP<sup>C</sup> protein in U87 and U251 WT and KO cells, in monolayer (M) and neurosphere (N) conditions (left) and analysis of the expression of PrP<sup>C</sup> in WT cells through band densitometry (right). Ratio between PrP<sup>C</sup> and Actin ( $n=3$ ;  $*P<0.05$ ;  $**P<0.001$ ;  $***P<0.0001$ ;  $****P<0.0001$ ). **(d)** Histogram of cell surface expression of PrP<sup>C</sup> in U87 WT and KO neurosphere cells, and in U251 WT and KO monolayer cells. **(e)** Heatmaps depicting the relative gene expression of stem cell markers in U87 and U251 KO monolayer cells and WT and KO neurosphere cells, in relation to their monolayer WT counterparts. Asterisks (\*) represent a comparison with the monolayer WT group, and plus signs (+) represent a comparison with the neurosphere WT group ( $p$  values are described in the Results section). **(f)** Histograms of cell surface expression of CD133 and SSEA1 proteins in U87 WT and PrP<sup>C</sup> KO neurospheres. **(g)** Growth curve of U87 and U251 WT and KO cells in monolayer condition ( $n=6$ ) ( $*p<0.05$ ,  $**p<0.01$ ,  $***p<0.001$ ,  $****p<0.0001$  comparing WT vs. KO of the same cell line;  $++++p<0.0001$  comparing U87 WT vs. U251 WT cells). **(h)** Self-renewal assays measuring the number of neurospheres in U87 and U251 WT and KO cells ( $n=**P<0.05$ ;  $**P<0.01$ )

PrP<sup>C</sup>-KO cells grown as neurospheres had decreased expression of *SOX2* ( $p=0.0038$ ) and *EGFR* ( $p=0.0238$ ) in comparison to WT neurospheres. In U251 PrP<sup>C</sup>-KO cells, the overall expression profile of stem cell markers was different than in U87 KO cells. In monolayer U251 KO cells, expression of *CD44* ( $p=0.0003$ ), *CD24* ( $p=0.001$ ), and *SOCS3* ( $p=0.0187$ ) were decreased relative to WT monolayer. Interestingly, expression of *SOX2* ( $p=0.0412$ ) and *SOCS3* ( $p<0.0001$ ) increased in WT

neurospheres, while *CD133* ( $p=0.0304$ ) decreased due to the culture conditions. U251 KO cells grown as neurospheres had reduced expression of *CD44* ( $p=0.0003$ ) in comparison with their WT neurosphere counterpart.

Additionally, loss-of-PrP<sup>C</sup> decreased cell surface protein expression of CD133 and SSEA1 in U87 KO cells grown as neurospheres (Fig. 1f). Functionally, PrP<sup>C</sup> KO cells showed decreased proliferation (Fig. 1g) and impaired capacity of GSCs self-renewal (Fig. 1h and

Additional Fig. 1d and e) in both cell lines. Together, these results provide an in-depth validation of our study model and show that the loss-of-PrP<sup>C</sup> affected the expression of GSCs markers and decreased the proliferative capacity of the cells in both cell lines.

#### Transcriptome analysis of U87 and U251 PrP<sup>C</sup>-KO cells reveals enrichment of pathways related to cell motility, proliferation and stemness

To elucidate the impact of PrP<sup>C</sup> depletion in intracellular pathways, we performed bulk transcriptome analysis of both PrP<sup>C</sup> KO cell lines (U87 and U251) grown in monolayer condition. Comparison between WT and KO cells yielded 1295 differentially expressed genes (DEGs) for U87 KO cells, and 363 DEGs for U251 KO cells (Fig. 2a-c). Among the DEGs found, there were the GSC markers *CD24* and *SOX2* (Fig. 2b), which had already been analyzed by qPCR (Fig. 1e). Moreover, overrepresentation analysis using different databases such as WikiPathways and Gene Ontology (GO) identified focal adhesion, regulation of neuron migration, and differentiation pathways to be overrepresented in U87 DEGs (Fig. 2d). For U251 DEGs, overrepresented pathways consisted of cell migration and invasion regulation, cell-cell adhesion, cell-matrix adhesion, and glial cell differentiation (Fig. 2d). As expected, we found several genes related to cell proliferation and invasion. Some genes of interest that are involved with cell adhesion, migration and GSCs biology were selected for further mRNA expression analysis through qPCR (Fig. 2d). Interestingly, once again, we observed a different expression profile between the cell lines. In U87 PrP<sup>C</sup>-KO cells, we found *EGF* ( $p=0.0007$ ), *WNT10B* ( $p=0.006$ ), and *ABCB5* ( $p<0.0001$ ) to be upregulated, while *EPHB4* ( $p=0.0201$ ), and *TIMP3* ( $p=0.016$ ) were found to be downregulated. On the other hand, in U251 PrP<sup>C</sup>-KO cells, we found *ABCB5* ( $p<0.0001$ ), *EGF* ( $p<0.0001$ ), *THBS2* ( $p=0.0009$ ), *NCAM1* ( $p=0.0003$ ), and *TIMP3* ( $p=0.0006$ ) to be downregulated, while *EPHA4* ( $p=0.0352$ ) was upregulated. Overall, the data obtained indicates that PrP<sup>C</sup> may have a role in the modulation of pathways related to cell proliferation, stemness, and migration, albeit some of the individual genes are different for each cell line.

#### PrP<sup>C</sup> modulates expression and localization of CD44

Given the role of PrP<sup>C</sup> as a scaffold protein and the abovementioned transcriptome analysis, it is imperative to uncover potential partners involved in the observed altered pathways. Given the established role of CD44 in cell motility and invasiveness, coupled with its previously reported interactions with PrP<sup>C</sup> in other tumor types [37–39], we hypothesized that CD44 may be implicated in the invasive characteristics of glioblastoma, prompting further investigation into its expression and functional

relationship with PrP<sup>C</sup> in our model. Although CD44 transcript levels remained unchanged in PrP<sup>C</sup> KO cells, CD44 protein levels were reduced in KO monolayer U251 cells, but not in U87 KO cells. In contrast, under neurosphere conditions, both U87 and U251 KO cells exhibited decreased CD44 protein levels. It is well known that discrepancies between mRNA and protein levels can arise from complex post-transcriptional and post-translational regulations [40–42]. CD44 protein levels showed a reduction in KO monolayer U251 cells, but not in U87 KO, while in the neurosphere condition, both U87 and U251 KO presented decreased levels of CD44 protein (Fig. 3a). In Fig. 3b, we observed a significant increase in PrP<sup>C</sup> levels in cells overexpressing CD44, suggesting that CD44 may modulate PrP<sup>C</sup> expression. Flow cytometry assays showed a decrease of CD44 on the cell surface of U87 PrP<sup>C</sup>-KO cells (Additional Fig. 1f). Additionally, immunofluorescence assays showed that PrP<sup>C</sup> and CD44 co-localize in filopodia-like structures on the cell membrane (Fig. 3c and d). The formation of such membrane protrusions is an important step in cell motility [29], and the decrease of their presence in KO cells might impair cell migration. Interestingly, we can also observe that PrP<sup>C</sup>-KO cells present sites of CD44 concentration, appearing as CD44 assemblies (Fig. 3c). Taken together, these data suggest that PrP<sup>C</sup> modulates the protein levels and membrane localization of CD44. Given the results obtained so far and the role of CD44 in cell migration, we decided to investigate the motility potential of KO cells. Indeed, transwell assays showed that the migration capabilities of KO cells were impaired in both monolayer cell lines (Fig. 3e and f) and neurospheres of U87 cells (Fig. 3g). We also observed impaired invasion in both PrP<sup>C</sup>-KO monolayer cell lines (Fig. 3e, f). Additionally, we investigated the invasive capacity of both WT and PrP<sup>C</sup>-KO GBM cells after CD44 overexpression. Our findings indicate that CD44 overexpression does not enhance the invasive potential of PrP<sup>C</sup>-KO cells. Consistent with previous findings (Fig. 3e-g), PrP<sup>C</sup>-KO cells exhibited lower invasiveness compared to their WT counterparts, further emphasizing the role of PrP<sup>C</sup> in promoting invasiveness (Fig. 3h). These results corroborate our RNA-seq findings and further consolidate the role of PrP<sup>C</sup> in glioblastoma motility.

#### Single-cell RNA sequencing analysis from patient-derived GBM cells corroborates PrP<sup>C</sup> significance in GSCs migration and proliferation

To deepen the insights obtained through experiments in U87 and U251 cell lines and further corroborate our results, we analyzed patient-derived data from bulk and single-cell RNA-seq (scRNA-Seq). These data were publicly available in Gliovis, The Cancer Genome Atlas (TCGA) Program GBM dataset, and the Broad Institute

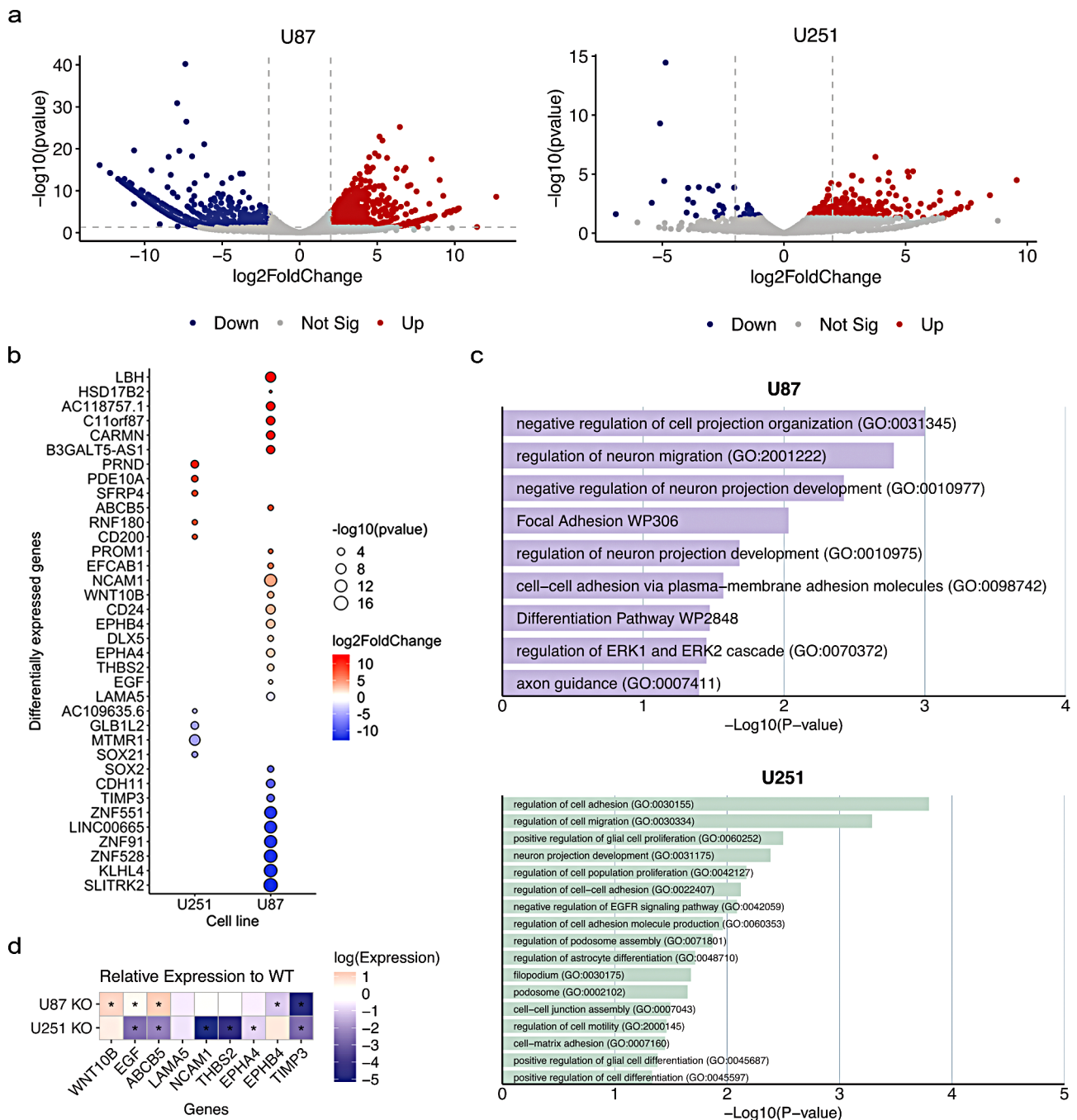


**Fig. 2** Bulk RNA-Seq data analysis shows that PrP<sup>C</sup> may modulate migration, proliferation, and stemness-related genes. **(a)** Volcano plots of the comparison between U87 and U251 WT versus PrP<sup>C</sup>-KO cells. The plots depict non-significant (gray), downregulated (blue), and upregulated (red) differentially expressed genes (DEGs). **(b)** Dot plot of key DEGs found in U87 and U251 cells, with size and color relating to *p*-value and fold change, respectively. **(c)** Overrepresentation analysis of U87 cells and U251 DEGs. **(d)** Gene expression of selected DEGs related to stemness maintenance, cellular migration, and invasion in U87 and U251 KO monolayer cells, in relation to their monolayer WT counterparts (p values are described in the Results section)

of Single-Cell Data Portal. Analysis of GBM patient samples from TCGA showed a positive correlation between *PRNP* and *CD44*, and with genes associated with stemness, including *CD133*, *SOX2*, and *EGFR* (Fig. 4a). Survival analysis from TCGA showed that GBM tumors with high expression of *PRNP* had decreased survival

in comparison to tumors with low *PRNP* expression (Fig. 4b). We also compared survival data between high- and low-*CD44* expressing tumors, but there was no difference between the groups (Fig. 4b). Correlation analysis of TCGA samples revealed significant associations between *PRNP* and *CD44* in mesenchymal and proneural

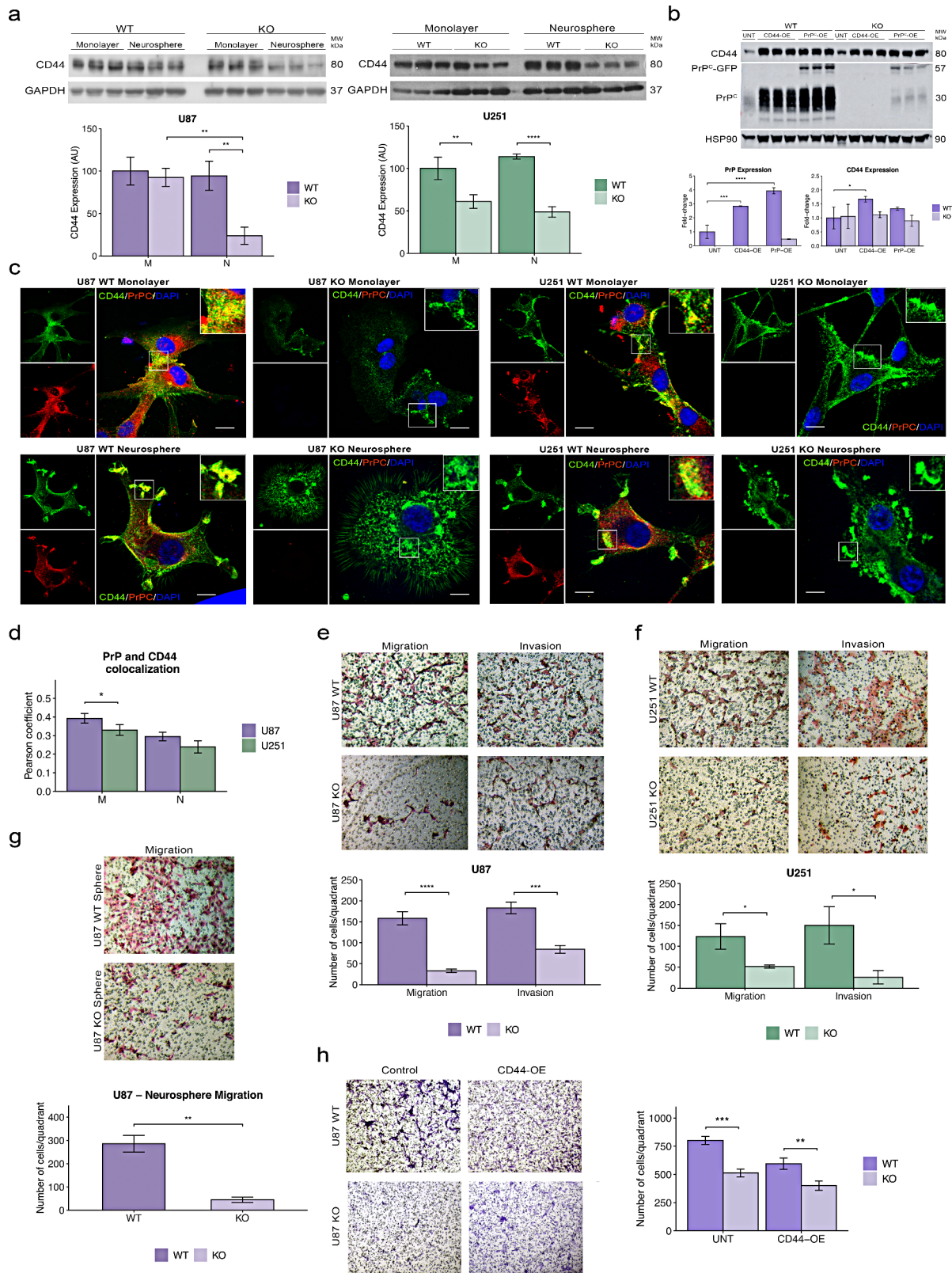


**Fig. 3** (See legend on next page.)

(See figure on previous page.)

**Fig. 3** Loss-of-PrP<sup>C</sup> disrupts CD44 expression and localization and decreases cell invasiveness. **(a)** Protein levels of CD44 in U87 and U251 WT and KO cells in monolayer and neurosphere conditions. Analysis of the expression of CD44 through band densitometry, with the ratio between CD44 and GAPDH. **(b)** Western blot analysis showing elevated PrP<sup>C</sup> levels in CD44-overexpressing cells. Densitometric analysis of PrP<sup>C</sup> and HSP90 (loading control) was performed for U87 WT and PrP<sup>C</sup> knockout (KO) cells transfected with CD44-GFP or PrP<sup>C</sup>-GFP (untransfected cells as control). Statistical analysis was conducted using a two-way ANOVA followed by Bonferroni's post-hoc test ( $n = 3$ ; \*\*\*\* $p < 0.0001$ , \*\*\* $p < 0.001$ ). **(c)** Immunofluorescence of CD44 (green), PrP<sup>C</sup> (red), and DAPI (blue) in U87 and U251 WT and KO monolayer and neurosphere conditions. Inserts in WT show co-localization of CD44 and PrP<sup>C</sup>. Inserts panel in KO shows CD44 assemblies, Scale bar = 15  $\mu\text{m}$ . **(d)** Pearson's correlation coefficient was calculated to quantify colocalization between CD44 and PrP<sup>C</sup> signals, with values presented in the graph. **(e-g)** Representative photomicrographs of U87 and U251WT and KO in monolayer and neurosphere conditions, for cellular migration or invasion through transwell assays, and graphical representation of the number of cells that migrated per quadrant. \* $p < 0.05$ ; \*\* $p < 0.01$ ; \*\*\* $p < 0.001$ ; \*\*\*\* $p < 0.0001$ . **(h)** Invasion assays confirmed previous findings, showing that PrP<sup>C</sup> KO reduces invasiveness in GBM cells, both in untransfected (UNT) and CD44-overexpressing conditions. A general decrease in cell invasion was observed in both WT and KO cells following CD44 transfection (\* $p < 0.05$ )

glioblastoma subtypes, suggesting potential co-regulatory mechanisms that could impact tumorigenic processes and cellular behavior in GBM (Fig. 4c-e). Additionally, we interrogated *PRNP* expression in 10,536 GSCs grown as neurospheres (Fig. 4f, g). Gene set enrichment analysis (GSEA) of cluster 10, the cluster with the highest *PRNP* expression, showed an upregulation of migration and proliferation pathways (Fig. 4h-j). Data found in this analysis indicates that PrP<sup>C</sup> may have a role in the modulation of key pathways related to the invasiveness of GBM, and further strengthens the findings described in this study.

## Discussion

GBM is one of the most aggressive cancer types, and its diffuse growth pattern plays a pivotal role in therapeutic failure since this tumor relies heavily on the ability of its cells to migrate and invade the brain parenchyma [43]. Proteins located on the cell surface are critical for cell migration, and, therefore, can contribute to tumor invasiveness. A deeper understanding of the formation and activity of multiprotein cell surface platforms involved in cell motility mechanisms is an effective way to identify novel potential therapeutic targets for GBM due to their accessibility and involvement with crucial signaling pathways. Not surprisingly, a growing body of evidence highlights the involvement of PrP<sup>C</sup> in cell migration, particularly in cancer [18]. We previously reported that the decrease in PrP<sup>C</sup> expression was enough to modulate membrane expression of key proteins involved in GBM invasion, such as E-cadherin and  $\alpha 6$ -integrin [19]. Herein, we show a central function of PrP<sup>C</sup> as a possible regulator of CD44 and signaling modules on the cell membrane related to cell motility, proliferation, and stemness in GBM.

Although PrP<sup>C</sup> and CD44 are known to interact physically and functionally in breast cancer cells (20), data exploring the correlation between PrP<sup>C</sup> and CD44 expression and its role in GBM cells is lacking. The most recent review by Thellung et al. [44] briefly mentions the insufficiency of studies exploring their functional interaction in GBM. We report herein that loss-of-PrP<sup>C</sup> leads to a decrease in CD44 protein levels in GSCs (Fig. 3c). When

we dissected the cellular distribution of CD44, we found that it co-localizes with PrP<sup>C</sup> in filopodia-like structures (Fig. 3d). Those structures are important for cell migration [45], and it is known that an essential characteristic of GBM is its ability to migrate through the brain tissue, hampering the complete removal of the tumor and, therefore, contributing to recurrence [46]. In PrP<sup>C</sup>-KO cells, loss-of-PrP<sup>C</sup> altered the distribution pattern of CD44 on the cell membrane. As CD44 was described to interact with PrP<sup>C</sup> physically and functionally on the cell surface of breast cancer cells [20], PrP<sup>C</sup> may be necessary for the proper localization of CD44 on the cellular membrane. Given the important role that CD44 has in cell migration and invasion in gliomas [39], the disruption of its location on the cell surface might also be related to the impairment of the migration and invasion we observed in PrP<sup>C</sup>-KO cells.

CD44 is one of the main partners of hyaluronic acid, and its proper interaction has been described as a necessary step for migration in lymphoma [37] and glioma [39]. Unlike solid organs, the brain is a softer tissue, and its extracellular matrix (ECM) composition differs significantly. The elasticity of brain tumors was shown to be higher than normal brain tissue [47]. Preclinical models also supported these findings, showing that heterogeneous GBM tissues become softer as hypoxic/necrotic regions develop, while denser areas with abnormal vascular components become stiffer [48]. The differences in tissue stiffness at the molecular level in GBM are attributed to changes in ECM composition. Increased levels of hyaluronic acid are detected in the tumor's surrounding ECM. This increased hyaluronic acid content promotes ECM remodeling and invasion of GBM cells [49]. Through in vitro biochemical studies, it has been determined that the morphology and migratory patterns of GBM cells exhibit an inverse relationship with the density of hyaluronic acid [50], and that the interaction between hyaluronic acid and its receptor CD44 plays a significant role in glioma invasion. Furthermore, the findings indicate that decreased hyaluronic acid levels contribute to enhanced flexibility [51], potentially facilitating the degradation of the neighboring ECM by

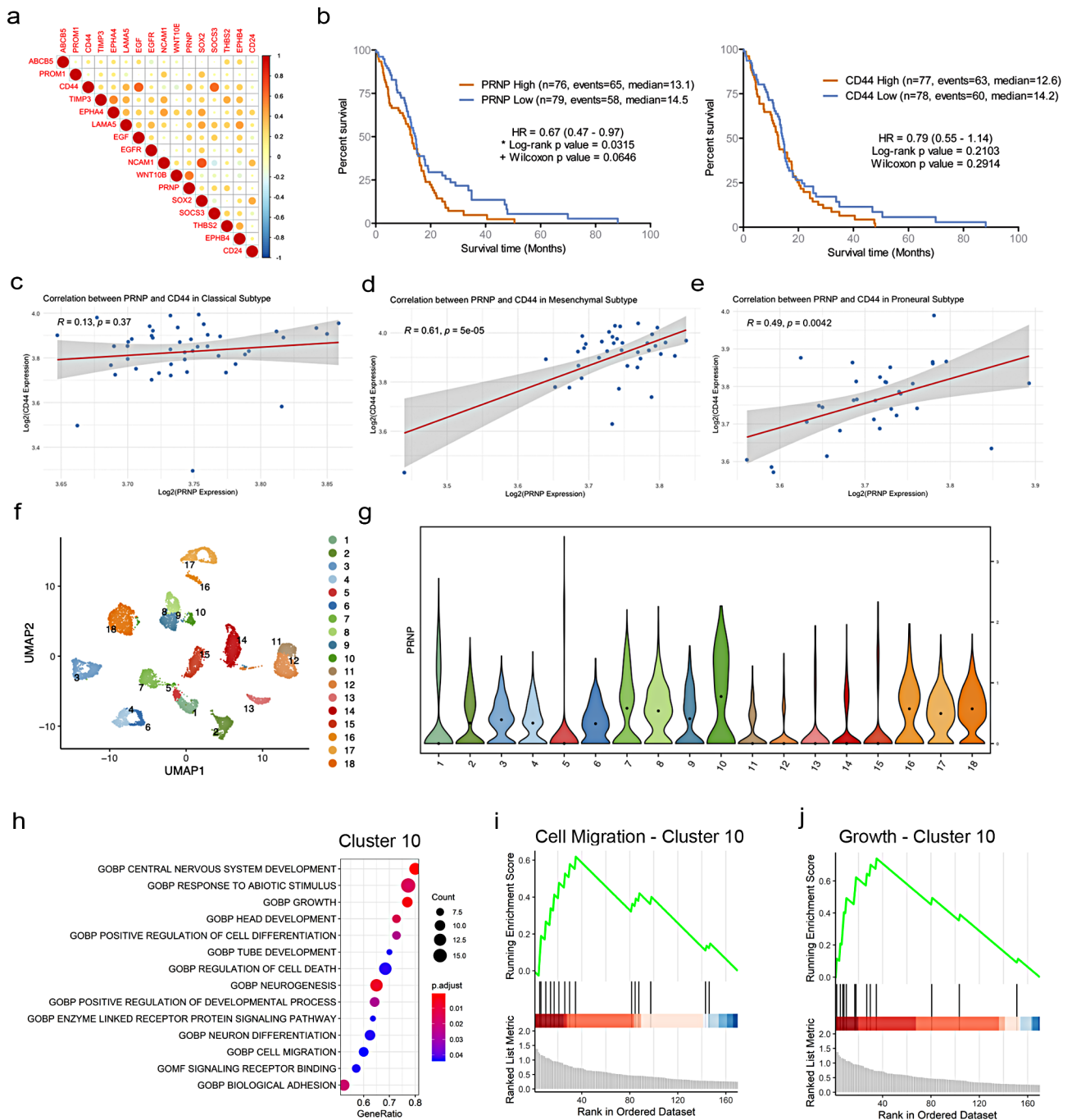


**Fig. 4** PRNP expression in patient tumor samples predicts lower survival and may be associated with migration and invasion pathways in glioblastoma stem cells. **(a)** Correlation between PRNP expression and GCS's regulators obtained from the TCGA database. **(b)** Curves showing survival probabilities in patients with varying PRNP (right) or CD44 expression (left). Survival and expression data were obtained from Gliovis, using the TCGA GBM dataset. **(c-e)** correlation analysis between CD44 and PRNP expression in GBM subtype samples. Scatter plot illustrating the relationship between CD44 and PRNP. The line represents the best-fit linear regression, with the Pearson correlation coefficient ( $r$ ) and significance level ( $p$ -value) indicated in the top left corner. **(f)** t-distributed stochastic neighbor embedding (UMAP) graphic showing GSCs cultivated as spheres ( $n=10,536$ ) distributed according to transcription patterns. Different colors represent each. **(g)** Violin plot shows PRNP expression in each cluster. Central dots represent the means. **(h)** Gene Set Enrichment Analysis (GSEA) of cluster 10 showing main upregulated pathways. **(i-j)** Enrichment score of cell migration-related pathways **(i)** and cell growth-related pathways **(j)**

matrix metalloproteinases (such as MMP2, MMP9, and MMP13). Consequently, this degradation enables tumor cells to invade the surrounding brain tissue [52]. Additionally, PrP<sup>C</sup> was shown to bind to glycosaminoglycans, among them hyaluronic acid [53]. Therefore, the decreased invasive capability of GBM PrP<sup>C</sup>-KO cells that we showed herein may be due to the disruption of this interaction between hyaluronic acid, CD44, and PrP<sup>C</sup>.

RNA-seq data analysis efficiently screened novel pathways and genes affected by the lack of PrP<sup>C</sup>. We confirmed that many of the DEGs in PrP<sup>C</sup> KO were related to cell migration. We found that EPHB4 and TIMP3 were downregulated in U87 PrP<sup>C</sup>-KO cells (Fig. 2d). Conversely, in U251 PrP<sup>C</sup>-KO, EPHA4, NCAM1, THBS2 and TIMP3 were all downregulated. Ephrin receptors, such as EPHB4 and EPHA4, are receptor tyrosine kinases that are overactivated in invasive GBM cells compared to cells in the tumor core. Phosphorylation of EPHB4 inhibits glioma migration and invasion [54]. EPHA4 promotes proliferation and migration in GBM by forming a complex with FGFR1 and subsequent modulation of Rac1 and Cdc42 [55]. Interestingly, PrP<sup>C</sup> has also been implicated in the modulation of Rac1 expression in cancer [30]. Additionally, both EPHA4 and EPHB4 are modulators of  $\beta$ 1-integrin expression [53, 54], and PrP<sup>C</sup> is known to regulate integrin signaling [56, 57]. Furthermore, literature shows that loss-of-PrP<sup>C</sup> expression leads to a disturbance in the expression of Eph receptors *in vitro* and *in vivo* [58]. In breast cancer tissues and cell lines, THBS2 is upregulated, and it was shown to facilitate cell migration and invasion [59]. NCAM1 mediates cell adhesion in neural cells, it can regulate migration and proliferation in cancer cells [60, 61], and it is a binding partner of PrP<sup>C</sup> [62]. Another DEG, TIMP3, regulates migration and invasion in osteosarcoma [63]. Interestingly, although U87 and U251 cell lines had different expression profiles in response to the lack of PrP<sup>C</sup>, both cell lines showed the same functional decrease in cell migration, invasion, and proliferation. This supports the importance of PrP<sup>C</sup> for GBM, as it demonstrates the same cellular functional output in different signaling and genetic environments. Importantly, the role of PrP<sup>C</sup> on GBM migration and invasion was also corroborated by our scRNA-seq analysis of GSCs.

In addition to being an essential modulator of GBM invasion, CD44 is discussed as a marker of GSCs and has a role in GBM growth [64]. Many of the DEGs we explored related to stemness in GBM present a correlation with CD44. ABCB5 is co-expressed with CD44 in oral cancer stem cells [65] and, as CD44, also presents an important role in breast cancer invasion and metastasis [38, 66]. In gliomas, expression of ABCB5 correlated with CD133 expression on primary GBM tumors, and ABCB5 was also found to be expressed on U87, LN-18,

and LN-229 GSCs that were positive for CD133 [67]. CD24 has emerged as a marker of neural progenitor-like GSCs, which are shown to be highly proliferative cells in IDH-mutant gliomas [68], and is often used together with CD44 as a marker for isolation of breast cancer stem cells [69]. Additionally, WNT10B is known to modulate cell growth and apoptosis in glioma [70] and is able to regulate stemness of CD44<sup>+</sup>/CD24<sup>-</sup> cells in breast cancer [71]. Not only that, but CD44 is also found to be a target of the Wnt/ $\beta$ -catenin pathway [72], and PrP<sup>C</sup> was shown to modulate Wnt signaling in intestinal epithelial cells [73].

Moreover, we reported a loss of membrane-bound SSEA-1 in U87 PrP<sup>C</sup>-KO cells (Fig. 1f), a neural stem cell marker [74], suggesting that PrP<sup>C</sup>-KO cells might have a more differentiated phenotype than their WT counterparts, strengthening the importance of PrP<sup>C</sup> in the biology of GSCs. In contrast to its increased mRNA expression, we also observed a decrease of membrane-bound CD133 in U87 PrP<sup>C</sup>-KO cells (Fig. 1f), in accordance with what was reported in U87 PrP<sup>C</sup> knockdown cells previously by our group [19]. Furthermore, we also observed a loss of expression of SOX2 in U87 PrP<sup>C</sup>-KO cells (Fig. 1e). SOX2 is a promoter of GBM stemness [75] and, together with CD44, is a marker of cancer stem cells in Epstein-Barr virus-positive nasopharyngeal carcinoma [76]. Additionally, knockdown of PrP<sup>C</sup> was previously shown to decrease SOX2 staining in U87 cells [19]. Regarding DEGs related to stemness maintenance, we once again observed a different expression profile between U87 and U251 PrP<sup>C</sup>-KO cells. These cell lines have different genetic backgrounds, functional behavior and recapitulate different aspects of GBM *in vivo* [77, 78]. U87 forms large vascularized tumors with a lack of necrotic cores. They also express mutant PTEN, are methylated by Methylguanine-DNA methyltransferase (MGMT), and have upregulated PI3K/Akt, but present wild-type TP53. U251 cells, on the other hand, form small, highly infiltrative tumors *in vivo*. They express mutant PTEN and TP53, are MGMT methylated, and show upregulation of the PI3K/Akt pathway [77]. Despite these diverse genetic and behavioral backgrounds, loss-of-PrP<sup>C</sup> equally decreased GBM proliferation and GSCs renewal in both models.

In this study, we have uncovered a novel role of PrP<sup>C</sup> in regulating the expression and localization of CD44. Moreover, our findings highlight the crucial involvement of PrP<sup>C</sup> in the migration and invasion processes of GBM, which are critical factors contributing to its dismal survival rates (Fig. 5). The diffuse growth pattern observed in GBM is a significant hurdle in effective treatment strategies, as it relies heavily on the migratory and invasive capabilities of tumor cells within the brain parenchyma [43]. Our RNA-Seq analysis identified numerous genes

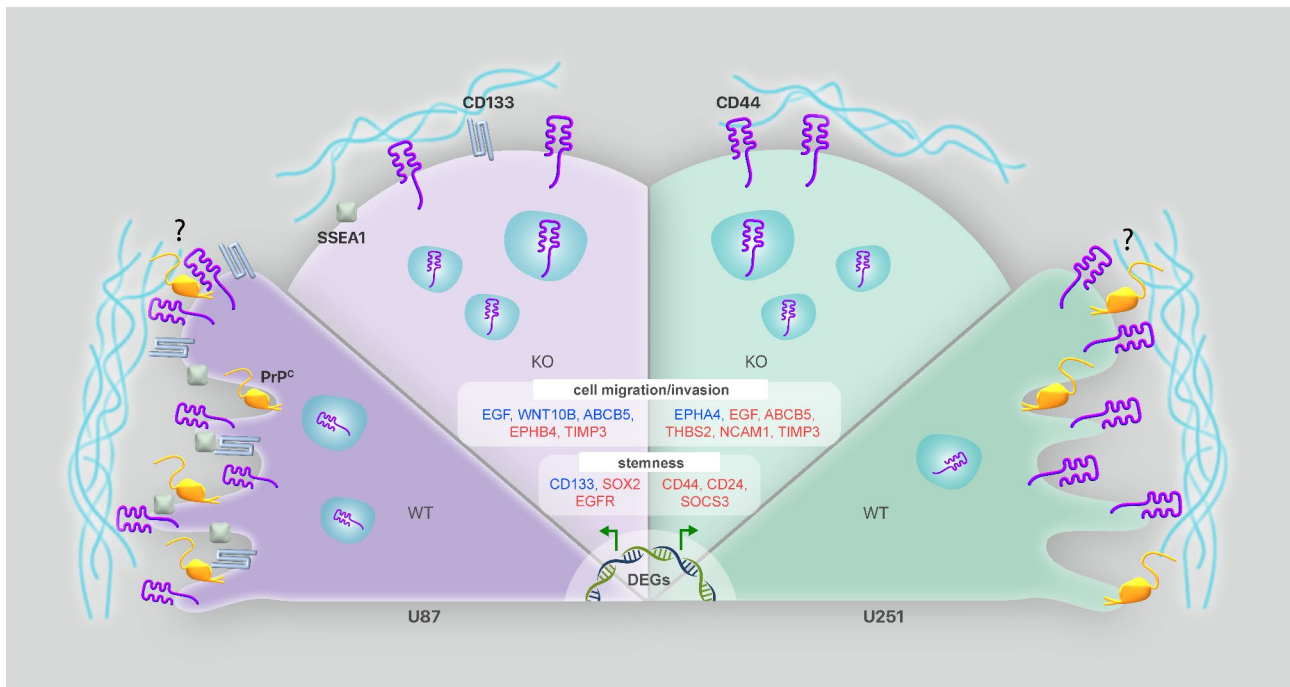


**Fig. 5** PrP<sup>C</sup> knockout impairs the invasiveness of glioblastoma. PrP<sup>C</sup> knockout (KO) in glioblastoma cells altered the expression of genes involved in cell migration, invasion, and stemness pathways. Notably, the cell lines U87 and U251 showed distinct expression patterns of these genes but had similar phenotypic responses to PrP<sup>C</sup>-KO, i.e., decreased proliferation, self-renewal, and migration and invasion capabilities. We also found that PrP<sup>C</sup>-KO led to a decrease in total protein levels of CD44 and of cell surface levels of SSEA1, CD44, and CD133. We propose that the lack of PrP<sup>C</sup> leads to a disruption of the interaction between CD44 and extracellular matrix components that impair GBM cell motility

modulated by PrP<sup>C</sup> expression in GBM cells, revealing their involvement in migration, proliferation, and stemness pathways. Remarkably, our study demonstrates that the loss-of-PrP<sup>C</sup> expression impairs GBM proliferation and the self-renewal abilities of GSCs, underscoring its functional significance in maintaining stemness. Though the majority of our experiments were performed in vitro, it's paramount to highlight that our bulk RNA-Seq data aligns with the single-cell analysis of GBM patients' cells, further reinforcing the pivotal role exerted by PrP<sup>C</sup> in GBM biology and strongly suggesting that our findings could be transposable to an in vivo setting. As a scaffold protein, the absence of PrP<sup>C</sup> may disrupt the formation of crucial signaling platforms on the cell surface, thereby disturbing vital molecule-molecule interactions and signaling pathways relevant to GBM. Moving forward, investigating the complex interactions between PrP<sup>C</sup>, CD44, and ECM components like hyaluronic acid holds great promise for gaining deeper insights into the critical role of PrP<sup>C</sup> in GBM.

## Conclusions

In summary, our study demonstrates that PrP<sup>C</sup> influences genes associated with migration, proliferation, and stemness pathways in GBM cells. The loss-of-PrP<sup>C</sup> expression impairs GBM cell proliferation, GSC self-renewal, migration, and invasion, highlighting its critical role in GBM

biology. These findings enhance the significance of PrP<sup>C</sup> in regulating key functions in GBM and GSC biology, positioning it as a compelling and novel target for future anti-glioblastoma therapeutic strategies.

## Abbreviations

bFGF	Basic fibroblast growth factor
DEGs	Differentially expressed genes
ECM	Extracellular matrix
EGF	Epidermal growth factor
EGFR	Epidermal growth factor receptor
GBM	Glioblastoma
GSCs	Glioblastoma stem cells
GSEA	Gene set enrichment analysis
IDH	Isocitrate dehydrogenase
MGMT	Methylguanine-DNA methyltransferase
NCAM1	Neural cell adhesion molecule 1
PrP <sup>C</sup>	Cellular prion protein
PrP <sup>C</sup> -KO	PrP <sup>C</sup> knockout
TCGA	The Cancer Genome Atlas
TMZ	Temozolomide

## Supplementary Information

The online version contains supplementary material available at <https://doi.org/10.1186/s12885-024-13285-4>.

Additional Figure 1: File containing Schematic representation of the *PRNP* gene, highlighting the primer alignments in specific regions. Alignment of the wild-type (WT) *PRNP* gene sequence from U87 cells and knockout (KO) clones generated using CRISPR-Cas9, with the CRISPR guide RNA sequence highlighted. Graphs of Extreme Limiting Dilution Analysis (ELDA) performed to estimate the frequency of stem-like cells in U87 cultures. Flow cytometry analysis histogram of CD44 expression in U87 WT and KO

cells.

Supplementary Material 2

### Acknowledgements

We are very grateful to Marlene Bernardes for technical assistance, as well as Dr. Chao Yun Irene Yan for kindly providing the PX330 plasmid. We also thank Martin Roff   for assistance with guide RNA design and Dr. Raphael B. Parmigiani for invaluable assistance with RNA sequencing.

### Author contributions

M.B.P. and M.H.L. conceived the study and designed experiments; M.B.P., R.P.I., R.N.A., B.P.C., and M.I.M-E. performed experiments; M.B.P., B.P.C. and M.C.C. analyzed data; F.M.F., J.M.B. and S.A. performed bioinformatics analysis; M.B.P., B.P.C., R.P.I., T.G.S., F.H.B., M.A.M.P., V.F.P., M.L.D. and M.H.L. analyzed and discussed the results; M.I.M-E designed illustrations; M.B.P. and B.P.C. designed the figures; J.F. assisted with PrPC sequencing and qPCR; M.B.P., B.P.C. and M.H.L. wrote the manuscript; M.B.P., B.P.C., R.P.I., R.N.A., J.M.B., C.F.L.F., M.I.M-E., S.A., T.G.S., F.H.B., J.F., F.M.F., H.I.N., M.A.M.P., V.F.P., M.L.D. and M.H.L. revised the manuscript.

### Funding

This research was funded by Funda  o de Amparo   Pesquisa do Estado de S o Paulo (FAPESP; 2017/26158-0 and 2018/19517-7 to M.B.P., 2019/14952-0 to B.P.C., 2020/03714-8 and 2019/12710-9 to R.P.I., 2022/08198-3 to R.N.A., 2020/07450-5 to J.M.B., 2019/14741-9 to C.F.L.F., 2019/11097-1 to M.I.M.E., 2017/20271-0 and 2018/15557-4 to M.H.L. and Conselho Nacional de Desenvolvimento Cient fico e Tecnol gico (101796/2020-0 to J.M.B., and 409941/2021-2, 307677/2022-2 and 406258/2022-8 to M.H.L.). Work performed at The University of Western Ontario received internal support via a FAPESP-Western collaborative grant and NSERC support (03592 – 2021 RGPIN; 06711–2019 RGPIN).

### Data availability

Count and transcript per million gene expression matrices, differentially expressed genes tables, as well as gene ontology (GO) and functional pathways (KEGG) tables generated for this study can be downloaded from the project's GitHub repository (<https://github.com/marilenehohmuth/PrionGBM>). Raw FastQ files can be downloaded from SRA (Sequence Read Archive). The data will be made publicly accessible through the following link <https://www.ncbi.nlm.nih.gov/sra/PRJNA1188731> (SRA- BioProject ID PRJNA1188731). All custom scripts, pipelines, and code used in data processing and figure creation will be available on the project's GitHub repository (<https://github.com/marilenehohmuth/PrionGBM>).

### Declarations

#### Ethical approval

Not applicable.

#### Consent to participate

Not applicable.

#### Consent for publication

Not applicable.

#### Competing interests

The authors declare no competing interests.

#### Author details

<sup>1</sup>Laboratory of Neurobiology and Stem Cells, Department of Cell and Developmental Biology, Institute of Biomedical Sciences, University of S o Paulo, S o Paulo, SP, Brazil

<sup>2</sup>The Donnelly Centre, University of Toronto, Toronto, Ontario, Canada

<sup>3</sup>Princess Margaret Cancer Centre, University Health Network, Toronto, Ontario, Canada

<sup>4</sup>Core Facility to Support Research - Institute of Biomedical Sciences (CEFAP), S o Paulo, Brazil

<sup>5</sup>Laboratory of Cell and Molecular Biology, International Research Center, A.C. Camargo Cancer Center, S o Paulo, SP, Brazil

<sup>6</sup>Robarts Research Institute, Departments of Physiology and Pharmacology, Anatomy and Cell Biology, and Biochemistry, The University of Western Ontario, London, Ontario, Canada

<sup>7</sup>Schulich School of Medicine & Dentistry, Department of Pathology and Laboratory Medicine, The University of Western Ontario, London, Ontario, Canada

<sup>8</sup>LIM50, Division of Pathology, University of S o Paulo School of Medicine, S o Paulo, Brazil

<sup>9</sup>Department of Clinical and Toxicological Analyses, School of Pharmaceutical Sciences, University of S o Paulo, S o Paulo, Brazil

<sup>10</sup>Scientific Platform Pasteur, University of S o Paulo, S o Paulo, Brazil

<sup>11</sup>Hospital Israelita Albert Einstein, S o Paulo, Brazil

Received: 31 May 2024 / Accepted: 3 December 2024

Published online: 18 December 2024

### References

- Louis DN, Perry A, Wesseling P, Brat DJ, Cree IA, Figarella-Branger D, Hawkins C, Ng HK, Pfister SM, Reifenberger G, et al. The 2021 WHO classification of tumors of the Central Nervous System: a summary. *Neuro Oncol*. 2021;23(8):1231–51.
- Paw I, Carpenter RC, Watabe K, Debinski W, Lo HW. Mechanisms regulating glioma invasion. *Cancer Lett*. 2015;362(1):1–7.
- Velasquez C, Mansouri S, Mora C, Nassiri F, Suppiah S, Martino J, Zadeh G, Fernandez-Luna JL. Molecular and Clinical Insights into the Invasive Capacity of Glioblastoma Cells. *J Oncol* 2019, 2019:1740763.
- Lathia JD, Mack SC, Mulkearns-Hubert EE, Valentim CL, Rich JN. Cancer stem cells in glioblastoma. *Genes Dev*. 2015;29(12):1203–17.
- Gimple RC, Bhargava S, Dixit D, Rich JN. Glioblastoma stem cells: lessons from the tumor hierarchy in a lethal cancer. *Genes Dev*. 2019;33(11–12):591–609.
- Brown DV, Filiz G, Daniel PM, Hollande F, Dworkin S, Amiridis S, Kountouri N, Ng W, Morokoff AP, Mantamadiotis T. Expression of CD133 and CD44 in glioblastoma stem cells correlates with cell proliferation, phenotype stability and intra-tumor heterogeneity. *PLoS ONE*. 2017;12(2):e0172791.
- Garros-Regulez L, Garcia I, Carrasco-Garcia E, Lantero A, Aldaz P, Moreno-Cugnon L, Arrizabalaga O, Undabeitia J, Torres-Bayona S, Villanua J, et al. Targeting SOX2 as a therapeutic strategy in Glioblastoma. *Front Oncol*. 2016;6:222.
- Westphal M, Maire CL, Lamszus K. EGFR as a target for Glioblastoma Treatment: an unfulfilled Promise. *CNS Drugs*. 2017;31(9):723–35.
- Crivii CB, Bosca AB, Melincovici CS, Constantin AM, Marginean M, Dronca E, Sufletel R, Gonciar D, Bungardean M, Sovrea A. Glioblastoma Microenvironment and Cellular interactions. *Cancers (Basel)* 2022, 14(4).
- Hersh AM, Gaiatsch H, Alomari S, Lubelski D, Tyler BM. Molecular pathways and genomic Landscape of Glioblastoma Stem cells: opportunities for targeted therapy. *Cancers (Basel)* 2022, 14(15).
- Frosina G. Limited advances in therapy of glioblastoma trigger re-consideration of research policy. *Crit Rev Oncol Hematol*. 2015;96(2):257–61.
- Strobel H, Baisch T, Fitzel R, Schilberg K, Siegelin MD, Karpel-Massler G, Debatin KM, Westhoff MA. Temozolomide and other Alkylating agents in Glioblastoma Therapy. *Biomedicines* 2019, 7(3).
- Yasaswi PS, Shetty K, Yadav KS. Temozolomide nano enabled medicine: promises made by the nanocarriers in glioblastoma therapy. *J Control Release*. 2021;336:549–71.
- Wulf MA, Senatore A, Aguzzi A. The biological function of the cellular prion protein: an update. *BMC Biol*. 2017;15(1):34.
- Martins VR, Beraldo FH, Hajj GN, Lopes MH, Lee KS, Prado MA, Linden R. Prion protein: orchestrating neurotrophic activities. *Curr Issues Mol Biol*. 2010;12(2):63–86.
- Linden R. The Biological function of the prion protein: a cell Surface Scaffold of Signaling modules. *Front Mol Neurosci*. 2017;10:77.
- Santos TG, Lopes MH, Martins VR. Targeting prion protein interactions in cancer. *Prion*. 2015;9(3):165–73.
- Prado MB, Melo Escobar MI, Alves RN, Coelho BP, Fernandes CFL, Boccacino JM, Iglesias RP, Lopes MH. Prion Protein at the Leading Edge: Its Role in Cell Motility. *Int J Mol Sci* 2020, 21(18).
- Iglesias RP, Prado MB, Cruz L, Martins VR, Santos TG, Lopes MH. Engagement of cellular prion protein with the co-chaperone Hsp70/90 organizing protein regulates the proliferation of glioblastoma stem-like cells. *Stem Cell Res Ther*. 2017;8(1):76.

20. Cheng Y, Tao L, Xu J, Li Q, Yu J, Jin Y, Chen Q, Xu Z, Zou Q, Liu X. CD44/cellular prion protein interact in multidrug resistant breast cancer cells and correlate with responses to neoadjuvant chemotherapy in breast cancer patients. *Mol Carcinog*. 2014;53(9):686–97.
21. Chen C, Zhao S, Karnad A, Freeman JW. The biology and role of CD44 in cancer progression: therapeutic implications. *J Hematol Oncol*. 2018;11(1):64.
22. Koliopoulos C, Ali MM, Castillejo-Lopez C, Heldin CH, Heldin P. CD44 depletion in Glioblastoma cells suppresses growth and stemness and induces senescence. *Cancers (Basel)* 2022, 14(15).
23. Yang C, Cao M, Liu Y, He Y, Du Y, Zhang G, Gao F. Inducible formation of leader cells driven by CD44 switching gives rise to collective invasion and metastases in luminal breast carcinomas. *Oncogene*. 2019;38(46):7113–32.
24. Xu H, Niu M, Yuan X, Wu K, Liu A. CD44 as a tumor biomarker and therapeutic target. *Exp Hematol Oncol*. 2020;9(1):36.
25. Bernardino-Sgherri J, Siberchicot C, Auvre F, Busso D, Brocas C, El Masri G, Lioutsko A, Ferri F, Radicella JP, Romeo PH, et al. Tumor resistance to radiotherapy is triggered by an ATM/TAK1-dependent-increased expression of the cellular prion protein. *Oncogene*. 2021;40(19):3460–9.
26. Kubota H, Yamamoto S, Itoh E, Abe Y, Nakamura A, Izumi Y, Okada H, Iida M, Nanjo H, Itoh H, et al. Increased expression of co-chaperone HOP with HSP90 and HSC70 and complex formation in human colonic carcinoma. *Cell Stress Chaperones*. 2010;15(6):1003–11.
27. Li QQ, Sun YP, Ruan CP, Xu XY, Ge JH, He J, Xu ZD, Wang Q, Gao WC. Cellular prion protein promotes glucose uptake through the Fyn-HIF-2 $\alpha$ -Glut1 pathway to support colorectal cancer cell survival. *Cancer Sci*. 2011;102(2):400–6.
28. Corsaro A, Bajetto A, Thellung S, Begani G, Villa V, Nizzari M, Pattarozzi A, Solari A, Gatti M, Pagano A, et al. Cellular prion protein controls stem cell-like properties of human glioblastoma tumor-initiating cells. *Oncotarget*. 2016;7(25):38638–57.
29. Gil M, Kim YK, Kim KE, Kim W, Park CS, Lee KJ. Cellular prion protein regulates invasion and migration of breast cancer cells through MMP-9 activity. *Biochem Biophys Res Commun*. 2016;470(1):213–9.
30. Lin SC, Lin CH, Shih NC, Liu HL, Wang WC, Lin KY, Liu ZY, Tseng YJ, Chang HK, Lin YC, et al. Cellular prion protein transcriptionally regulated by NF13 enhances lung cancer cell lamellipodium formation and migration through JNK signaling. *Oncogene*. 2020;39(2):385–98.
31. Lopes MH, Santos TG, Rodrigues BR, Queiroz-Hazrabassanov N, Cunha IW, Wasilewska-Sampaio AP, Costa-Silva B, Marchi FA, Bleggi-Torres LF, Sanematsu PI, et al. Disruption of prion protein-HOP engagement impairs glioblastoma growth and cognitive decline and improves overall survival. *Oncogene*. 2015;34(25):3305–14.
32. Ryskalin L, Biagioni F, Busceti CL, Giambelluca MA, Morelli L, Frati A, Fornai F. The role of Cellular prion protein in promoting stemness and differentiation in Cancer. *Cancers (Basel)* 2021, 13(2).
33. Kondo T, Setoguchi T, Taga T. Persistence of a small subpopulation of cancer stem-like cells in the C6 glioma cell line. *Proc Natl Acad Sci U S A*. 2004;101(3):781–6.
34. Singh SK, Clarke ID, Terasaki M, Bonn VE, Hawkins C, Squire J, Dirks PB. Identification of a cancer stem cell in human brain tumors. *Cancer Res*. 2003;63(18):5821–8.
35. Etoc F, Metzger J, Ruzo A, Kirst C, Yoney A, Ozair MZ, Brivanlou AH, Siggia ED. A balance between secreted inhibitors and Edge sensing Controls Gastruloid Self-Organization. *Dev Cell*. 2016;39(3):302–15.
36. Livak KJ, Schmittgen TD. Analysis of relative gene expression data using real-time quantitative PCR and the 2 $^{-\Delta\Delta C_T}$  method. *Methods*. 2001;25(4):402–8.
37. Alaniz L, Cabrera PV, Blanco G, Ernst G, Rimoldi G, Alvarez E, Hajos SE. Interaction of CD44 with different forms of hyaluronic acid. Its role in adhesion and migration of tumor cells. *Cell Commun Adhes*. 2002;9(3):117–30.
38. Nam K, Oh S, Lee KM, Yoo SA, Shin I. CD44 regulates cell proliferation, migration, and invasion via modulation of c-Src transcription in human breast cancer cells. *Cell Signal*. 2015;27(9):1882–94.
39. Okada H, Yoshida J, Sokabe M, Wakabayashi T, Hagiwara M. Suppression of CD44 expression decreases migration and invasion of human glioma cells. *Int J Cancer*. 1996;66(2):255–60.
40. Wei YN, Hu HY, Xie GC, Fu N, Ning ZB, Zeng R, Khaitovich P. Transcript and protein expression decoupling reveals RNA binding proteins and miRNAs as potential modulators of human aging. *Genome Biol*. 2015;16(1):41.
41. Fortelny N, Overall CM, Pavlidis P, Freue GVC. Can we predict protein from mRNA. Levels? *Nat*. 2017;547(7664):E19–20.
42. Jiang D, Cope AL, Zhang J, Pennell M. On the Decoupling of Evolutionary Changes in mRNA and protein levels. *Mol Biol Evol* 2023, 40(8).
43. Claes A, Idema AJ, Wesseling P. Diffuse glioma growth: a guerilla war. *Acta Neuropathol*. 2007;114(5):443–58.
44. Thellung S, Corsaro A, Bosio AG, Zambito M, Barbieri F, Mazzanti M, Florio T. Emerging role of Cellular prion protein in the maintenance and expansion of glioma stem cells. *Cells* 2019, 8(11).
45. Jacquemet G, Hamidi H, Ivaska J. Filopodia in cell adhesion, 3D migration and cancer cell invasion. *Curr Opin Cell Biol*. 2015;36:23–31.
46. Liu CA, Chang CY, Hsueh KW, Su HL, Chiou TW, Lin SZ, Harn HJ. Migration/ Invasion of Malignant gliomas and implications for Therapeutic Treatment. *Int J Mol Sci* 2018, 19(4).
47. Chauvet D, Imbault M, Capelle L, Demene C, Mossad M, Karachi C, Boch AL, Gennissou JL, Tanter M. In vivo measurement of Brain Tumor elasticity using intraoperative Shear Wave Elastography. *Ultraschall Med*. 2016;37(6):584–90.
48. Schregel K, Nazari N, Nowicki MO, Palotai M, Lawler SE, Sinkov R, Barbone PE, Patz S. Characterization of glioblastoma in an orthotopic mouse model with magnetic resonance elastography. *NMR Biomed*. 2018;31(10):e3840.
49. Perrin SL, Samuel MS, Koszyca B, Brown MP, Ebert LM, Oksdath M, Gomez GA. Glioblastoma heterogeneity and the tumour microenvironment: implications for preclinical research and development of new treatments. *Biochem Soc Trans*. 2019;47(2):625–38.
50. Rao SS, Dejesus J, Short AR, Otero JJ, Sarkar A, Winter JO. Glioblastoma behaviors in three-dimensional collagen-hyaluronan composite hydrogels. *ACS Appl Mater Interfaces*. 2013;5(19):9276–84.
51. Chen JE, Pedron S, Harley BAC. The combined influence of Hydrogel stiffness and matrix-bound Hyaluronic Acid Content on Glioblastoma Invasion. *Macromol Biosci* 2017, 17(8).
52. Manini I, Caponnetto F, Bartolini A, Ius T, Mariuzzi L, Di Loreto C, Beltrami AP, Cesselli D. Role of Microenvironment in Glioma Invasion: what we learned from in Vitro models. *Int J Mol Sci* 2018, 19(11).
53. Pan T, Wong BS, Liu T, Li R, Petersen RB, Sy MS. Cell-surface prion protein interacts with glycosaminoglycans. *Biochem J*. 2002;368(Pt 1):81–90.
54. Kawahara Y, Furuta T, Sabit H, Tamai S, Dong Y, Jiapaer S, Zhang J, Zhang G, Oishi M, Miyashita K, et al. Ligand-dependent EphB4 activation serves as an anchoring signal in glioma cells. *Cancer Lett*. 2019;449:56–65.
55. Fukai J, Yokote H, Yamanaka R, Arai T, Nishio K, Itakura T. EphA4 promotes cell proliferation and migration through a novel EphA4-FGFR1 signaling pathway in the human glioma U251 cell line. *Mol Cancer Ther*. 2008;7(9):2768–78.
56. Ghodrati F, Mehrabian M, Williams D, Halgas O, Bourkas MEC, Watts JC, Pai EF, Schmitt-Ulms G. The prion protein is embedded in a molecular environment that modulates transforming growth factor beta and integrin signaling. *Sci Rep*. 2018;8(1):8654.
57. Hajj GN, Lopes MH, Mercadante AF, Veiga SS, da Silveira RB, Santos TG, Ribeiro KC, Juliano MA, Jacchieri SG, Zanata SM, et al. Cellular prion protein interaction with vitronectin supports axonal growth and is compensated by integrins. *J Cell Sci*. 2007;120(Pt 11):1915–26.
58. Hirsch TZ, Martin-Lannere S, Reine F, Hernandez-Rapp J, Herzog L, Dron M, Privat N, Passet B, Halliez S, Villa-Diaz A, et al. Epigenetic control of the notch and eph signaling pathways by the prion protein: implications for Prion diseases. *Mol Neurobiol*. 2019;56(3):2159–73.
59. Qi L, Sun B, Yang B, Lu S. CEBPB regulates the migration, invasion and EMT of breast cancer cells by inhibiting THBS2 expression and O-fucosylation. *Hum Mol Genet*. 2023;32(11):1850–63.
60. Li J, Yang R, Yang H, Chen S, Wang L, Li M, Yang S, Feng Z, Bi J. NCAM regulates the proliferation, apoptosis, autophagy, EMT, and migration of human melanoma cells via the Src/Akt/mTOR/cofilin signaling pathway. *J Cell Biochem*. 2020;121(2):1192–204.
61. Yang B, Huang S, Chen H, Li R, Hou S, Zhao J, Li Y. DNMT3B regulates proliferation of A549 cells through the microRNA-152-3p/NCAM1 pathway. *Oncol Lett*. 2022;23(1):11.
62. Miranzadeh Mahabadi H, Taghibiglou C. Cellular Prion Protein (PrPc): Putative Interacting Partners and Consequences of the Interaction. *Int J Mol Sci* 2020, 21(19).
63. Han XG, Li Y, Mo HM, Li K, Lin D, Zhao CQ, Zhao J, Tang TT. TIMP3 regulates osteosarcoma cell migration, invasion, and chemotherapeutic resistances. *Tumour Biol*. 2016;37(7):8857–67.
64. Mooney KL, Choy W, Sidhu S, Pelargos P, Bui TT, Voth B, Barnette N, Yang I. The role of CD44 in glioblastoma multiforme. *J Clin Neurosci*. 2016;34:1–5.
65. Grimm M, Krimmel M, Polligkeit J, Alexander D, Munz A, Kluba S, Keutel C, Hoffmann J, Reinert S, Hoefert S. ABCB5 expression and cancer

- stem cell hypothesis in oral squamous cell carcinoma. *Eur J Cancer*. 2012;48(17):3186–97.
66. Yao J, Yao X, Tian T, Fu X, Wang W, Li S, Shi T, Suo A, Ruan Z, Guo H, et al. ABCB5-ZEB1 Axis promotes Invasion and Metastasis in breast Cancer cells. *Oncol Res*. 2017;25(3):305–16.
  67. Lee CAA, Banerjee P, Wilson BJ, Wu S, Guo Q, Berg G, Karpova S, Mishra A, Lian JW, Tran J, et al. Targeting the ABC transporter ABCB5 sensitizes glioblastoma to temozolomide-induced apoptosis through a cell-cycle checkpoint regulation mechanism. *J Biol Chem*. 2020;295(22):7774–88.
  68. Suva ML, Tirosh I. The glioma stem cell model in the era of single-cell Genomics. *Cancer Cell*. 2020;37(5):630–6.
  69. Jaggupilli A, Elkord E. Significance of CD44 and CD24 as cancer stem cell markers: an enduring ambiguity. *Clin Dev Immunol* 2012, 2012:708036.
  70. Liu Y, Yaozu Z, Zhao H, Peng P, Tingbao Z, Jincan C. Inhibition of Glioma Cell Growth and apoptosis induction through Targeting Wnt10B expression by Pyrazolo[4,3-c]pyridine-4-one. *Med Sci Monit*. 2020;26:e923912.
  71. Li X, Chen W, Huang L, Zhu M, Zhang H, Si Y, Li H, Luo Q, Yu B. Sinomenine hydrochloride suppresses the stemness of breast cancer stem cells by inhibiting wnt signaling pathway through down-regulation of WNT10B. *Pharmacol Res*. 2022;179:106222.
  72. Xu X, Zhang M, Xu F, Jiang S. Wnt signaling in breast cancer: biological mechanisms, challenges and opportunities. *Mol Cancer*. 2020;19(1):165.
  73. Besnier LS, Cardot P, Da Rocha B, Simon A, Loew D, Klein C, Riveau B, Lacasa M, Clair C, Rousset M, et al. The cellular prion protein PrPc is a partner of the wnt pathway in intestinal epithelial cells. *Mol Biol Cell*. 2015;26(18):3313–28.
  74. Mao XG, Zhang X, Xue XY, Guo G, Wang P, Zhang W, Fei Z, Zhen HN, You SW, Yang H. Brain Tumor Stem-Like cells identified by neural stem cell marker CD15. *Transl Oncol*. 2009;2(4):247–57.
  75. Berezovsky AD, Poisson LM, Cherba D, Webb CP, Transou AD, Lemke NW, Hong X, Hasselbach LA, Irtenkauf SM, Mikkelsen T, et al. Sox2 promotes malignancy in glioblastoma by regulating plasticity and astrocytic differentiation. *Neoplasia*. 2014;16(3):193–206. 206 e119-125.
  76. Lun SW, Cheung ST, Cheung PF, To KF, Woo JK, Choy KW, Chow C, Cheung CC, Chung GT, Cheng AS, et al. CD44 + cancer stem-like cells in EBV-associated nasopharyngeal carcinoma. *PLoS ONE*. 2012;7(12):e52426.
  77. Schulz JA, Rodgers LT, Kryscio RJ, Hartz AMS, Bauer B. Characterization and comparison of human glioblastoma models. *BMC Cancer*. 2022;22(1):844.
  78. Sesen J, Dahan P, Scotland SJ, Saland E, Dang VT, Lemarie A, Tyler BM, Brem H, Toulas C, Cohen-Jonathan Moyal E, et al. Metformin inhibits growth of human glioblastoma cells and enhances therapeutic response. *PLoS ONE*. 2015;10(4):e0123721.

### Publisher's note

Springer Nature remains neutral with regard to jurisdictional claims in published maps and institutional affiliations.